Tuberculosis Disease Classification on Thorax X-ray Images

Nyayu Chika Marselina**, Yullase Pratiwi**, Fawwaz Rif'at Revista**, Galih Prabasidi**

Department of Computer Science, Universitas Gadjah Mada,
Bulaksumur, Yogyakarta, Indonesia, 55281

nyayuchikamarselina@mail.ugm.ac.id
yullasepratiwi@mail.ugm.ac.id
fawwazrifatrevista@mail.ugm.ac.id
galih.prabasidi@mail.ugm.ac.id

***Abstract*— Tuberculosis (TBC) is an infectious disease that continues to pose a global health challenge, requiring early detection systems that are both effective and efficient. This study develops a tuberculosis classification system based on thoracic X-ray images using classical image processing techniques and machine learning algorithms. The preprocessing stage involves Gaussian filtering and CLAHE to enhance image quality and highlight lung structures. Lung segmentation is conducted using Otsu thresholding, flood fill, and morphological closing, producing a cleaner segmentation mask with an average IoU of 75.5%. Feature extraction employs GLCM, HOG, and LBP, followed by dimensionality reduction using PCA to minimize redundancy and improve model stability. Classification is performed using a Support Vector Machine (SVM), achieving an overall accuracy of 77%, a recall of 80% for the TBC class, and balanced F1-scores across both categories. These results demonstrate that classical image processing techniques combined with SVM can provide competitive performance in distinguishing between normal and TBC chest X-ray images. The proposed system shows potential as a lightweight diagnostic support tool, particularly for healthcare facilities with limited computational resources.**

***Keywords*— Tuberculosis, Chest X-ray, Image Segmentation, GLCM, LBP, HOG, *Support Vector Machine*.**

I. INTRODUCTION

A. Background

Tuberculosis (TBC) remains one of the most fatal infectious diseases worldwide. The World Health Organization (WHO) reported that prior to the COVID-19 pandemic, TBC was the leading cause of death from infectious diseases, with approximately 10 million new cases and 1.5 million deaths annually [1].

TBC infection can be identified through chest X-ray examinations. Chest radiography plays an essential role in early detection because it is relatively fast and inexpensive; however, its interpretation is highly dependent on the radiologist's expertise. This leads to inter-reader variability that can affect diagnostic consistency [1].

Another factor contributing to diagnostic inconsistency is the quality of the X-ray images used [2], [3]. Poor-quality radiographs increase the likelihood of diagnostic errors due to noise, low contrast, and uneven illumination. High-quality radiographic images are crucial for more effective detection of TBC infection [4]. Therefore, there is a need for methods that enhance X-ray image quality, commonly addressed through digital image processing.

Digital image processing provides an alternative solution by automating the analysis of chest radiographs. Classical machine learning techniques—through segmentation, feature extraction, and classification—can improve diagnostic accuracy without requiring deep learning models that demand large datasets and high computational resources. For instance, the Canny segmentation method has been used to distinguish between normal and abnormal lung images based on significant differences in pixel distribution [5].

Furthermore, studies show that the Histogram of Oriented Gradients (HOG) combined with the K-Nearest Neighbor (KNN) algorithm can identify pneumonia in chest X-ray images with accuracy exceeding 80% [6]. Similar approaches can be applied to TBC classification. Other methods, such as Local Binary Pattern (LBP) and Gray Level Co-occurrence Matrix (GLCM), have also proven effective as texture-based feature extraction techniques when combined with classifiers like Naive Bayes or Random Forest [7].

Recent research also demonstrates the success of non–deep learning methods. For example, [8] utilized Support Vector Machine (SVM), Logistic Regression, and Nearest Neighbor to detect TBC from radiographs with promising results. In addition, approaches involving morphological-based segmentation, feature extraction, and classification using Stacked Loopy Decision Trees (SLDT) have shown high accuracy [9], while Naive Bayes algorithms

have also been successfully applied following active contour segmentation for TBC classification [10].

As part of the Digital Image Processing course, this study focuses on implementing segmentation, feature extraction, and image classification techniques for medical applications, specifically TBC detection based on chest X-ray images. The approach integrates classical segmentation techniques such as thresholding and morphological operations with texture-based feature extraction methods including GLCM, HOG, and LBP. The extracted features are then analyzed using the SVM machine learning classifier. Thus, this study aims not only to produce an accurate and efficient TBC classification system but also to strengthen conceptual and practical understanding of digital image processing while contributing to technology-assisted disease detection.

B. Problem Formulation

Based on the background described previously, the problem formulation of this study is stated as follows:

1. This study focuses on designing a tuberculosis (TBC) classification system based on chest X-ray images using classical image processing techniques without employing deep learning approaches.
2. This study examines the lung segmentation process using classical methods to obtain a clean and well-separated lung mask from the background.
3. This study evaluates the feature extraction process of lung images to produce relevant texture and structural representations for classification.
4. This study assesses the application of the Support Vector Machine (SVM) algorithm as a classification model to distinguish between TBC and normal chest X-ray images.
5. This study measures the overall performance of the classification system using standard evaluation metrics, including accuracy, precision, recall, F1-score, and IoU.

C. Research Limitations

The implementation of image data processing in this study is limited by the following constraints:

1. The data used are limited to publicly available chest X-ray datasets and do not include clinical data obtained directly from hospitals.
2. The classification task is restricted to two categories only—TBC and normal (non-TBC) images—and does not cover other pulmonary diseases such as pneumonia or lung cancer.
3. The methods employed are limited to classical feature extraction techniques, including GLCM, HOG, and LBP.
4. The classification algorithm utilized in this study focuses solely on the Support Vector Machine (SVM) machine learning method.
5. The lung image segmentation process is limited to classical techniques widely used in previous studies, particularly thresholding-based methods; deep learning–based segmentation approaches are not applied.
6. This study does not employ any deep learning methods, as such approaches require large datasets and significant computational resources.

D. Research Objectives

The objectives of this study are as follows:

1. To develop a tuberculosis (TBC) classification system based on chest X-ray images using classical image processing techniques without applying deep learning approaches.
2. To design and implement a lung segmentation method using classical thresholding techniques in order to obtain clearer lung regions prior to feature extraction.
3. To perform lung image feature extraction using GLCM, HOG, and LBP in order to generate feature representations suitable for the classification process.
4. To apply a traditional classification algorithm, namely Support Vector Machine (SVM), to differentiate between TBC and non-TBC chest X-ray images.
5. To evaluate the performance of the classification system using standard metrics such as accuracy, precision, recall, F1-score, and IoU for assessing the developed model.

E. Research Benefits

This study is expected to contribute to the advancement of knowledge in the field of medical image processing, particularly in the application of classical machine learning–based segmentation and classification methods. Practically, the resulting system can serve as a lightweight and efficient diagnostic support tool, making it potentially suitable for implementation in healthcare facilities with limited computational resources. From a social perspective, this research may support efforts toward faster and more accurate early detection of tuberculosis, thereby helping to control the spread of the disease within the community.

II. Literature Review

A. *Tuberculosis* (TBC)

Tuberculosis (TB) is a chronic infectious disease transmitted directly from person to person and caused by the bacterium *Mycobacterium tuberculosis*. This disease typically attacks the lungs, regardless of age or gender. The pathogen is a highly resilient bacillus, requiring prolonged treatment due to its strong resistance. Although TB can infect various organs, the lungs are the most commonly affected, making pulmonary tuberculosis the most prevalent form of the disease in Indonesia [11].

According to WHO (World Health Organization) data, the number of tuberculosis cases in the Southeast Asia region reached 2,656,560 in 2015, while Indonesia alone recorded 6,375,585 cases (WHO Region, 2016). Diagnostic examinations for pulmonary TB may include the evaluation of clinical symptoms, culture testing, microscopic analysis, radiological examinations, and the tuberculin test. Early detection significantly improves treatment outcomes, reduces transmission, and helps control drug-resistant TB as well as multidrug-resistant TB [11].

One of the most frequently used diagnostic techniques is chest X-ray imaging. Each pulmonary disease exhibits distinct patterns and characteristics, including tuberculosis. However, diagnosis remains highly dependent on the clinician performing the assessment, making it subjective. Many individuals still regard prolonged cough as a common condition, whereas persistent coughing is one of the key symptoms of tuberculosis. Most patients seek medical attention only when their condition has worsened.

B. Preprocessing

1) *Contrast Limited Adaptive Histogram Equalization* (CLAHE)

CLAHE operates by determining a clipping threshold that defines the maximum height of the histogram and limits the extent of contrast enhancement [12]. According to [13], the CLAHE computation process utilizes a histogram clip limit. The clip limit can be calculated using Equation (1).

$$\beta = \frac{M}{N}\left(1 + \frac{\alpha}{100}(S_{max} - 1)\right) \quad (1)$$

where M represents the area size, N denotes the grayscale value, and α is the clip factor used to increase the histogram limit, with a range from 1 to 100.

2) Normalization

Normalization is the process of transforming the scale of attribute values within a dataset so that they fall within a specific range [14]. In this study, the data are normalized using the min–max normalization method. According to [15], the equation used for data normalization is presented in Equation (2).

$$X^* = \frac{X - \min(X)}{\max(X) - \min(X)} \quad (2)$$

where *min(X)* represents the minimum value, *max(X)* represents the maximum value, and X denotes the pixel intensity of the image data.

3) Gaussian Filter

The Gaussian filter is a widely used smoothing technique in image processing, known for its effectiveness in reducing noise. This filter is based on the Gaussian function, which produces smooth and natural blurring effects. The parameters of the Gaussian filter determine its behavior and the degree of smoothing applied. The primary purpose of using a Gaussian filter is to reduce high-frequency noise and produce a smoother image [16].

1. Kernel Size (Window Size): Determines the region of the image to be smoothed. A larger kernel size produces stronger smoothing but may blur fine details.
2. Standard Deviation (σ): Controls the spread of the Gaussian function.
3. Gaussian Function: A higher σ value increases the smoothing effect, reducing noise but potentially removing small details.
4. Kernel Shape: Typically square or circular, defining the area over which the Gaussian function is applied.
5. Dimensionality: The filter may be applied in 1D, 2D (for images), or 3D (for volumetric data).

4) Sobel Operator

Edge detection aims to enhance the appearance of boundaries within an image. The process involves identifying locations where pixel intensities exhibit significant discontinuities relative to their neighboring pixels. A point *(x, y)* is classified as an edge if it exhibits a large intensity difference compared to its surrounding pixels. The Sobel method is categorized as a first-order gradient operator. It was introduced by Irwin Sobel in 1970 and utilizes a pair of 3×3 kernels to compute gradients in the horizontal (**Gx**) and vertical (**Gy**) directions. These kernels (masks) are applied to detect intensity transitions, as illustrated in Figure 2.1 [17].

-1	-2	-1
0	0	0
1	2	1

G_x

-1	0	1
-2	0	2
-1	0	1

G_y

Figure 2.1. Kernel Sobel [17]

C. Segmentation

For objects with uniform intensity or color that are positioned against a background with distinct intensity or color, thresholding can be used for segmentation. Thresholding is performed by selecting a specific intensity or color value that separates the object from its background.One commonly used automatic thresholding technique is the Otsu method, which determines the optimal threshold by minimizing intra-class intensity variance. The chosen threshold is the one that results in the smallest within-class variance:

$$\sigma_W^2(t) = \omega_0(t)\sigma_0^2(t) + \omega_1(t)\sigma_1^2(t) \quad (3)$$

The weights ω_0 and ω_1 represent the probabilities of the data belonging to class 0 and class 1, respectively. Meanwhile, σ_0^2 and σ_1^2 denote the variances of each corresponding class. The Otsu method computes the within-class variance σ^2_w across all possible threshold values, from the lowest to the highest intensity level. The threshold that produces the smallest σ^2_w is selected as the optimal threshold [18].

D. Postprocessing

1) Flood Fill

Flood Fill is a classical algorithm in image processing used for region filling, which involves filling a specific area in an image based on pixel intensity similarity and connectivity. The algorithm operates by selecting a seed point and then coloring all connected pixels (either 4-connected or 8-connected) as long as their values remain within the defined range [19].

2) Morphological operations

Morphological operations are image processing techniques based on mathematical set theory, used to analyze and manipulate the shapes of objects in binary images. These operations work by applying a structuring element—a small template that determines the pixel pattern to be analyzed—to the image. The results of morphological operations depend on the shape and size of the structuring element used, which commonly takes the form of squares, circles, or crosses with varying sizes such as 3×3, 5×5, or 7×7 pixels [20].

Closing is a composite morphological operation consisting of dilation followed by erosion using the same structuring element. Closing is effective for filling small holes and gaps within an object while preserving the general shape and size of the main structure [20]. Mathematically, it can be expressed as follows:

$$A \bullet B = (A \oplus B) \ominus B \qquad (4)$$

Closing possesses several important properties, including smoothing object boundaries, connecting nearby separated components, and filling small concavities along the object's border.

E. Feature Extraction

1) *Gray Level Co-occurrence Matrix* (GLCM)

The Gray Level Co-occurrence Matrix (GLCM) is a feature extraction method used for texture analysis that produces a set of statistical measurements. This matrix is a two-dimensional square matrix that represents the spatial arrangement of neighboring pixels. It is constructed by counting the number of occurrences of specific pixel pair combinations within an image. The dimension of the GLCM is V_x X V_x where V_x denotes the number of grayscale levels present in each row of the image [21].

The GLCM can be generated based on various distances (displacements) and orientation angles, as illustrated in Figure 2.2, where the center pixel is considered the reference pixel. The distance between the reference pixel and its neighboring pixel is defined as the offset [21].

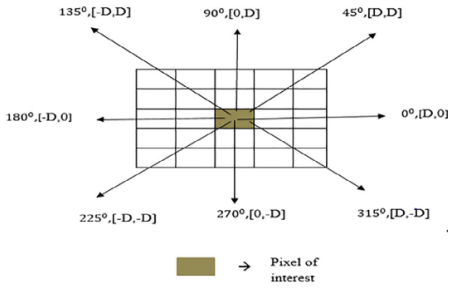

Figure 2.2. GLCM Orientation and Distance [21]

Multiple GLCM matrices can be constructed using different offsets, orientations, and displacements. Second-order statistical features derived from these GLCM matrices are computed as shown in Figure 2.3.

Angular second moment	$\sum_{m=1}^{M}\sum_{n=1}^{M}(mn)\,V(m,n)$
Contrast	$\sum_{m=1}^{M}\sum_{n=1}^{M}(m-n)^2\,V(m,n)$
Correlation	$\sum_{m=1}^{M}\sum_{n=1}^{M}\left(\frac{m-\mu}{\sigma}\right)\left(\frac{n-\mu}{\sigma}\right)V(m,n)$
Energy	$\sum_{m=1}^{M}\sum_{n=1}^{M}V(m,n)^2$
Homogeneity	$\sum_{m=1}^{M}\sum_{n=1}^{M}\frac{V(m,n)}{1+(m-n)^2}$
Dissimilarity	$\sum_{m=1}^{M}\sum_{n=1}^{M}\lvert m-n\rvert\,V(m,n)$
Difference variance	$\sum_{q=0}^{M-1}\left(q-\mu_{i-j}\right)^2 p_{i-j}(q)$
Difference entropy	$-\sum_{q=0}^{M-1}p_{i-j}(q)\log V_{i-j}$
Cluster side	$\sum_{m=1}^{M}\sum_{n=1}^{M}(m+n-2\mu)^4\,V(m,n)$
Cluster prominence	$\sum_{m=1}^{M}\sum_{n=1}^{M}(m+n-2\mu)^3\,V(m,n)$
Inverse difference	$\sum_{m=1}^{M}\sum_{n=1}^{M}\frac{V(m,n)}{1+\lvert m-n\rvert}$
Maximum probability	$max_{mn}V(m,n)$
Sum average	$\sum_{q=2}^{2M}q\,V_{i+j}(q)$
Sum entropy	$-\sum_{q=2}^{2M}p_{i+j}(q)\log V_{i+j}(q)$
Sum square	$\sum_{m=1}^{M}\sum_{n=1}^{M}(m-\mu)^2V(m,n)$

Figure 2.3. GLCM Statistical Features [21]

2) *Local Binary Pattern* (LBP)

Local Binary Pattern (LBP) is one of the widely used image feature extraction methods for texture analysis on grayscale images, which are subsequently converted into integer values. LBP is an image operation that transforms an image into an array of integer labels representing the micro-texture patterns within small neighborhoods of the image. The LBP operation compares the grayscale value of a central pixel with those of its neighboring pixels using a simple computational process. The pixel values of a grayscale image are taken from a 3×3 matrix. One of the advantages of the LBP method is its high tolerance to variations in grayscale intensity across individual pixels. LBP can be formulated as follows [22]:

$$LBP_{P,R} = \sum_{p=0}^{p-1} S(g_p - g_c)2^p \quad (5)$$

$$S(x) = \begin{cases} 1, & x \geq 0 \\ 0, & x < 0 \end{cases} \quad (6)$$

In Equation (5) of the LBP formulation, *R* represents the decimal value converted from the binary pattern, *P* denotes the number of sampling points, and *R* (radius) is the distance between the center pixel and its neighboring pixels. The term g□ refers to the grayscale value at sampling point *p*, while g⊂ refers to the grayscale value of the center pixel. In Equation (6), *S(x)* denotes the threshold function. The LBP process illustrated in Figure 2.4 can be described through the following steps:

1. Specify the LBP parameters to be used, namely *P* and *R*, where *P* is the number of sampling points or neighboring pixels, and *R* is the radius or distance between the center pixel and its neighboring pixels.
2. Compare each neighboring pixel value with the center pixel value to generate a binary value using the 3×3 matrix-based operation. This process is referred to as thresholding. A value of 0 is assigned if the neighboring pixel intensity is less than or equal to the center pixel intensity, whereas a value of 1 is assigned if it is greater. The mathematical definition of this comparison is given in Equation (6).
3. Multiply the thresholding results by an 8-bit weighting matrix, producing a series of weighted values that are then summed to generate the LBP integer value.
4. Represent the resulting decimal LBP values using a histogram, which displays the relative frequency of intensity occurrences within the image.

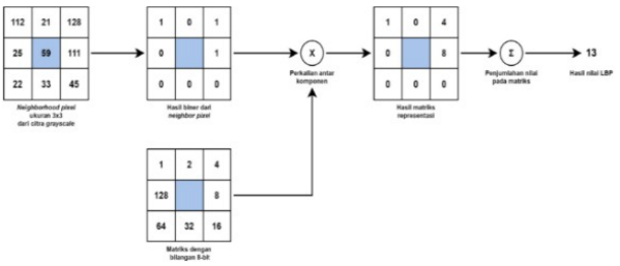

Figure 2.4. Steps for Computing Binary Values in LBP [22]

3) Histogram of Oriented Gradients (HOG)

HOG operates on the principle that the distribution of gradient intensities within localized regions is effective for characterizing object edges and shapes. The image is divided into cells that represent small, uniformly distributed regions to be compared. These cells are then grouped into blocks, which are subsequently normalized to maintain consistency against illumination variations or photometric effects. The features extracted from these normalized blocks form what is known as the Histogram of Oriented Gradients (HOG). The HOG feature extraction process consists of several key steps [23]:

1. Preprocessing (Normalization and Gamma/Color Adjustment)
   In this step, the image is resized and normalized to ensure consistent illumination and scale prior to feature extraction.
2. Gradient Computation
   The next step involves computing the image gradients to identify locations where pixel intensity changes significantly. These gradients highlight edges and structural details within the image.
3. Spatial / Orientation Binning
   The image is then divided into 8×8 cells, and gradients are computed for all pixels within each cell. For example, a 128×256 image contains 8 cells horizontally per row and 32 cells vertically per column. Each cell contains 8×8×3 = 192 pixels (in the case of RGB), and each pixel contributes gradient magnitude and orientation (two values), resulting in 8×8×2 = 128 gradient values per cell.
   The gradient magnitudes and orientations in each 8×8 block are represented using a 9-bin histogram.
4. Block Normalization
   Four adjacent cells (2×2) are grouped into a block and normalized to reduce the influence of illumination variations across the image. Neighboring blocks are compared to stabilize gradient features under different lighting conditions.
5. Constructing the HOG Feature Vector
   After computing all block normalizations, the resulting histograms are concatenated into a single feature vector, forming the one-dimensional HOG

descriptor representing the structural information in the image.

F. Classification

Support Vector Machine (SVM) is a technique that aims to identify the optimal separating function (classifier) among many possible functions to distinguish between two or more classes of objects. This separator is referred to as a *hyperplane*. The optimal hyperplane lies precisely between objects belonging to different classes. Maximizing the margin—defined as the perpendicular distance between the hyperplane and the support vectors—is essential for achieving the best separation. For data that are not linearly separable, SVM employs the *kernel trick*, which maps the data into a higher-dimensional space where linear separation becomes possible. Several commonly used kernel functions include [24] :

1. Linear Kernel : used when the data are linearly separable.
2. Polynomial Kernel : maps data into a higher-dimensional polynomial space.
3. Radial Basis Function (RBF) Kernel : effective for nonlinear data and widely used in image processing and classification tasks.

SVM is known for its ability to handle high-dimensional data and its robustness against overfitting, particularly in cases where the number of features exceeds the number of samples, as often encountered in medical image processing [24].

G. Evaluation

1) Confusion Matrix

The confusion matrix is an evaluation method that utilizes a tabular matrix commonly applied in data mining to calculate the accuracy of a model. Evaluation using the confusion matrix produces several metrics, including accuracy, precision, recall, and F1-score.

Accuracy measures how many of the model's predictions are correct relative to the total number of data points. Precision measures the proportion of predicted positive cases that are truly positive. Recall measures how many actual positive cases are successfully identified by the model. The F1-score represents the harmonic mean of precision and recall, providing a balanced assessment between the two [26].

2) Intersection over Union (IoU)

The performance of the segmentation model is evaluated using the quantitative metric Intersection over Union (IoU). IoU measures the ratio between the area of overlap and the area of union between the predicted mask and the ground truth. A high IoU value indicates that the model is capable of producing accurate segmentation results that closely match the expected reference output [27].

III. RESEARCH METODOLOGY

A. Data Sample

The dataset used in this study is a combined collection of chest X-ray images from the Montgomery and Shenzhen datasets, consisting of 704 samples obtained through Kaggle. The dataset contains two classes: label **1** for tuberculosis (TBC)-positive images and label **0** for normal or TBC-negative images. The dataset can be accessed at : https://www.kaggle.com/datasets/iamtapendu/chest-x-ray-lungs-segmentation.

B. *Preprocessing*

The preprocessing procedures performed in this study include downsampling, grayscale conversion, Gaussian filtering, and CLAHE. Downsampling is applied to reduce the image size to 256×256 pixels, ensuring that subsequent processing steps are computationally efficient. After downsampling, a Gaussian filter is applied, followed by CLAHE. These two processes are used to enhance the visibility of lung structures. CLAHE functions as a form of histogram equalization, and its effect enhances lung boundaries, thereby facilitating the segmentation process.

C. Segmentation

The segmentation process is performed to generate a mask used to separate the lung region (ROI) from the non-lung region (non-ROI). This process utilizes Otsu thresholding, flood fill with region growing, and morphological closing. Otsu thresholding separates the lung area from the rest of the body. Pixel intensities below the threshold (lung region) are set to *on*, while pixel intensities above the threshold (body region) are set to *off*.

Following Otsu thresholding, the background outside the body becomes *on* because its intensity values are similar to those of the lung area. Flood fill with region growing is then applied to assign *off* values to this outer region. For the region growing process, the image is padded by one pixel on all sides, and the seed point is initialized from the padded area.

Morphological closing is subsequently applied to unify separated lung components. After this step, the two largest connected regions are selected as the lung areas, resulting in the final lung mask.

D. Feature Extraction

The features of the segmented images are extracted for further analysis. The features used in this study include GLCM, LBP, HOG, Sobel, statistical features, and shape features. The GLCM features extracted consist of contrast, dissimilarity, homogeneity, energy, correlation, and ASM, while the orientations used for GLCM computation are 0°, 45°, 135°, 180°, 225°, and 315°.

The statistical features extracted include mean, standard deviation, skewness, and kurtosis. The shape features include area, perimeter, solidity, and eccentricity.

E. Feature Reduction and Classification

The extracted features are divided into training and testing subsets at a ratio of 8:2. Because the feature reduction and classification processes are sensitive to data scale, all extracted features are normalized to floating-point values ranging from 0 to 1 prior to further processing. After normalization, Principal Component Analysis (PCA) is applied to reduce feature redundancy and prevent model overfitting. Subsequently, lung image classification is performed using the Support Vector Machine (SVM) model. The PCA-reduced training features are used to train the SVM, while the PCA-reduced testing features are used to evaluate its performance. The SVM model classifies each image into either the *normal* class or the *TBC* class.

F.Evaluation Method

Two categories of metrics are evaluated in this study: segmentation performance and classification performance. For segmentation, the predicted mask produced by the segmentation process is compared with the ground-truth mask provided in the dataset by computing the Intersection over Union (IoU) between the two masks. For classification, the metrics assessed include accuracy, precision, sensitivity (recall), and the F1-score.

IV. Experimental Results and Discussion

This study employs a combined chest X-ray dataset from the Montgomery and Shenzhen collections, obtained from Kaggle. The dataset is labeled and evenly divided into two classes: TBC and normal. In total, the dataset consists of 704 X-ray images and 704 corresponding ground-truth masks. Prior to classification, preprocessing is performed by resizing all images to 256×256 pixels. The lung lesion regions are then enhanced using Gaussian filtering and CLAHE. The results of the preprocessing stage are presented in Table 4.1.

TABLE 4.1
Preprocessing Results on X-Ray Data
(a) Original Image (b) Gaussian Filter (c) CLAHE

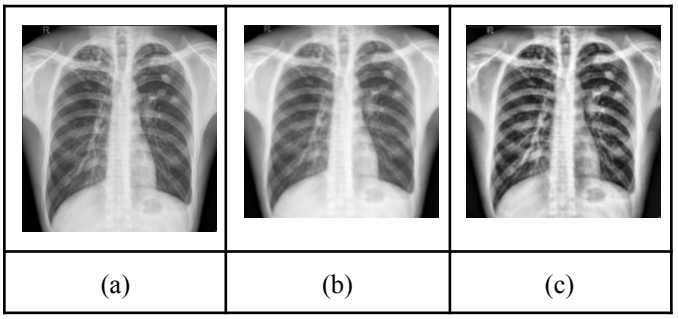

(a)	(b)	(c)

From Table 4.1, it can be seen that the lesion areas in the lungs become clearer. The details of the lungs appear more prominent, and the intensity differences between lung tissue and the background become more noticeable. After preprocessing, segmentation is performed using Otsu thresholding. Because X-ray images contain background regions, edge-cleaning is carried out using flood fill. Since there are still many holes within the lung areas, a morphological closing operation is applied to fill those gaps. The segmentation results can be seen in Table 4.2.

TABLE 4.2
Segmentation Results on X-Ray Data
(a) Otsu (b) *Flood Fill* (C) Closing Morphological

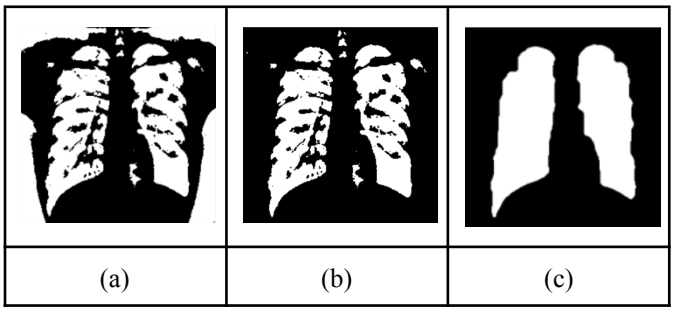

(a)	(b)	(c)

Based on Table 4.2, it can be observed that in image (a), the Otsu method produces a suboptimal segmentation result, as many irrelevant regions—such as bones and surrounding tissues—are still incorrectly segmented as part of the object. In addition, the lung shape produced is unclear, and a significant amount of noise remains in image (a). Image (b) shows an improvement over the Otsu result, where unwanted background regions have been removed. However, noise and holes within the lung area are still present. Image (c) presents a more refined segmentation result, where the holes previously found within the lung area and the noise surrounding the lungs have been corrected using morphological closing. The visual output in image (c) more closely resembles the true anatomical structure of the lungs, producing a much cleaner segmentation compared to the results obtained using only Otsu and flood fill.

The next stage after segmentation is feature extraction. The feature extraction methods used include GLCM, HOG, and LBP. The extracted features are then reduced using PCA. Subsequently, the dataset is split using an 80% training and 20% testing ratio. The training data are used to train the SVM model, with the PCA-reduced features serving as the input for SVM model training. After the SVM model is trained, it is evaluated using the test data to assess its performance in classifying normal and TBC images. The performance results of the SVM model are presented in Table 4.3.

TABLE 4.3
SVM Performance Results

Class	Accuracy	Precision	*Recall*	*F1-Score*	*IoU*
Normal	77%	79%	74%	76%	75.5%
TBC		74%	80%	77%	
Average	77%	76.5%	77%	76.5%	75.5%

Based on Table 4.3, the evaluation parameters used to assess the performance of the SVM model are accuracy, precision, recall, F1-score, and IoU. The SVM model achieved an accuracy of 77%, which means the model correctly predicted 77% of the total data, but there is still a 23% chance of error. The SVM model obtained a recall value of 80% for the TBC class, indicating that the model successfully detected patients who truly had tuberculosis, while its performance on the normal class was slightly lower compared to when recognizing the TBC class. The resulting F1-scores are relatively balanced, indicating that the model is not biased toward any particular class. However, optimization of features or parameters is still required to improve overall accuracy so that the model can detect tuberculosis more effectively.

V. Conclusion and Recommendations

Based on the conducted study, it can be concluded that the preprocessing stages using Gaussian filtering and CLAHE, combined with a multi-step segmentation process (Otsu thresholding, flood fill, and morphological closing), successfully enhanced the visibility of lung lesions and effectively separated the lung region from the background. This process proved to be effective, achieving an IoU of 75.5%, indicating that the lung segmentation was carried out with sufficient precision.

In the feature extraction stage, the combination of GLCM, HOG, and LBP produced informative representations of the image characteristics. Subsequently, feature selection and dimensionality reduction using PCA were applied to filter the most significant features and reduce redundancy. The use of PCA contributed to improving model stability and mitigating the risk of overfitting, as the features used became more focused and relevant.

The SVM classification model trained on PCA-reduced features demonstrated competitive performance, achieving an average accuracy of 77%. This model is considered effective for supporting medical diagnosis, as reflected in the recall value of 80% for the TBC class, indicating strong capability in detecting positive cases. Furthermore, the balanced F1-score shows that the model is not biased toward either class and is able to maintain consistent performance.

Nevertheless, there remains an error margin of approximately 23% that needs to be minimized. Therefore, further studies are recommended to optimize SVM hyperparameters, apply more specialized feature selection methods when necessary, or explore more advanced dimensionality reduction techniques to improve model performance. Increasing the amount of training data is also recommended to enhance the model's robustness in recognizing various chest X-ray image patterns.

References

[1] S. Hansun, et al., "Machine and deep learning for tuberculosis detection on chest X-rays: A systematic literature review," Appl. Sci., vol. 13, no. 2, pp. 1–26, 2023. doi: 10.3390/app13020781.

[2] S. Jaeger, A. Karargyris, S. Candemir, J. Siegelman, L. Folio, S. Antani et al., "Automatic screening for tuberculosis in chest radiographs: a survey," Quantitative Imaging in Medicine and Surgery, vol. 3, no. 2, pp. 89–99, 2013.

[3] A. M. Kanaya, D. V. Glidden, and H. F. Chambers, "Identifying pulmonary tuberculosis in patients with negative sputum smear results," Chest, vol. 120, no. 2, pp. 349–355, 2001.

[4] A. M. Ajlan, "Technical quality and diagnostic impact of chest X-rays in tuberculosis screening: Insights from a Saudi teleradiology cohort," Cureus, vol. 16, no. 2, 2024. doi: 10.7759/cureus.53509.

[5] R. Fauzi and D. Riana, "Metode segmentasi Canny pada citra rontgen," J. Nas. Tek. Elektro dan Teknol. Inf. (JNTETI), vol. 7, no. 3, pp. 277–282, 2018. doi: 10.22146/jnteti.v7i3.40839.

[6] D. M. Khairina, E. Sibarani, E. Muliono, R. W. Sembiring, and M. Muhathir, "Identification of pneumonia using the K-nearest neighbors method with HOG feature extraction," IOP Conf. Ser.: Mater. Sci. Eng., vol. 1211, no. 1, p. 012034, 2022. doi: 10.1088/1757-899X/1211/1/012034.

[7] R. A. Suaib and N. Tritosmoro, "Perbandingan performa metode Local Binary Pattern dan Random Forest dalam identifikasi COVID-19 pada citra X-ray paru-paru," J. Teknol. dan Sist. Komput., vol. 11, no. 1, pp. 39–46, 2023. doi: 10.14710/jtsiskom.2023.11.1.39-46.

[8] R. Alsaffar, A. Altaweel, and A. Hamad, "Detection of tuberculosis disease using image processing technique," J. Phys.: Conf. Ser., vol. 1804, no. 1, p. 012126, 2021. doi: 10.1088/1742-6596/1804/1/012126.

[9] X. A. Inbaraj, M. Villavicencio, J. J. Macrohon, S. S. Jeng, and J. G. Hsieh, "A novel machine learning approach for tuberculosis segmentation and prediction using chest-X-ray (CXR) images," Appl. Sci., vol. 11, no. 19, p. 9057, 2021. doi: 10.3390/app11199057.

[10] G. Pavani, S. Biswal, K. V. Sairam, and C. Subrahmanyam, "A semantic contour-based segmentation of lungs from chest X-rays for the classification of tuberculosis using Naïve Bayes classifier," Int. J. Intell. Syst. Appl. Eng., vol. 9, no. 3, pp. 83–90, 2021. doi: 10.18201/ijisae.2021.7639.

[11] [11] A. Rasyid and L. Heryawan, "Klasifikasi Penyakit Tuberculosis (TB) Organ Paru Manusia Berdasarkan Citra Rontgen Thorax Menggunakan Metode Convolutional Neural Network (CNN)," *Jurnal Manajemen Informasi Kesehatan Indonesia*, vol. 11, no. 1, pp. 35–45, 2023.

[12] F. Brinkmann, J. Hofgrefe, F. Ahrens, J. Weidemann, L. D. Berthold, N. Schwerk, *et al.*, "TB or not TB? Diagnostic sensitivity, specificity and interobserver agreement in the radiological diagnosis of pulmonary tuberculosis in children," *Klinische Pädiatrie*, vol. 236, no. 2, pp. 123–128, Feb. 2024. doi: 10.1055/a-2230-6958. PMID: 38320580.

[13] Tim Laboratorium Pengolahan Sinyal Digital, *Modul Praktikum Pengolahan Sinyal Digital*, Fakultas Elektro dan Komunikasi, Universitas Telkom, Bandung, 2009.

[14] S. Lazebnik, C. Schmid, and J. Ponce, "Beyond bags of features: Spatial pyramid matching for recognizing natural scene categories," in *Proc. IEEE Conf. Computer Vision and Pattern Recognition (CVPR)*, 2006. doi: 10.1109/CVPR.2006.68.

[15] D. G. Lowe, "Distinctive image features from scale-invariant keypoints," *International Journal of Computer Vision*, vol. 60, no. 2, pp. 91–110, 2004. doi: 10.1023/B:VISI.0000029664.99615.94.

[16] K. Kumar and B. T. Chakkaravarthy, "Contrast Enhancement and Noise Reduction Through Synthesizing Gaussian Filter, CLAHE and HE Algorithm for Image Preprocessing," in *Proc. 2025 International Conference on Emerging Technologies in Engineering Applications (ICETEA)*, pp. 1–10, 2025, doi: 10.1109/ICETEA64585.2025.11100055.

[17] M. Riyanto.Dasar Pengolahan Citra Digital. Edisi Revisi 2022. Jakarta: Penerbit Andi, 2022.

[18] A. Chithra and R. Roy R.U., "Otsu's adaptive thresholding based segmentation for detection of lung nodules in ct image," in 2018 2nd

International Conference on Trends in Electronics and Informatics (ICOEI), 2018, pp. 1303–1307.
[19] M. M. Alammar and M. Lopez-Benitez, “Enhanced signal area estimation based on edge detection and flood fill,” IEEE Access. vol. 10, pp. 47179–47194, 2022.
[20] M. Y. F., B. Yuwono, and D. B. P., *Dasar Pengolahan Citra Digital, Edisi 2022*. Yogyakarta: Lembaga Penelitian dan Pengabdian kepada Masyarakat, UPN Veteran Yogyakarta, 2022. ISBN: 978-6233-89144-8.
[21] P. G. Pavani, B. Biswal, M. V. S. Sairam, and N. B. Subrahmanyam, “A semantic contour based segmentation of lungs from chest x-rays for the classification of tuberculosis using Naïve Bayes classifier,” *International Journal of Imaging Systems and Technology*, pp. 1–15, 2021, doi: 10.1002/ima.22556.
[22] R. A. Suaib, N. Tritosmoro, and M. Ibrahim, "Identifikasi COVID-19 berdasarkan citra X-ray paru-paru menggunakan metode Local Binary Pattern dan Random Forest," *J. Rekayasa Elektrika*, vol. 18, no. 2, pp. 93–101, 2022. doi: 10.17529/jre.v18i2.21060.
[23] H. Leidiyana and J. Warta, “Implementasi Metode SVM untuk Klasifikasi Bunga dengan Ekstraksi Fitur Histogram of Gradient (HOG),” *Journal of Information and Information Security (JIFORTY)*, vol. 3, no. 1, pp. 89–98, Jun. 2022
[24] M. E. Affandy, M. Sofie, and M. Rofi’i, “Klasifikasi Penyakit Tumor Ginjal Menggunakan SVM dengan Ekstraksi Ciri HOG dan GLCM,” *The Indonesian Journal of Computer Science*, vol. 14, no. 3, pp. 4349–4361, Jun. 2025, doi: 10.33022/ijcs.v14i3.4882.
[25] N. Suhandi, R. Gustriansyah, and A. Destria, “Klasifikasi Penyakit TBC Menggunakan Metode UMAP dan K-NN,” *Bit-Tech (Binary Digital – Technology)*, vol. 7, no. 3, pp. 844–852, Apr. 2025, doi: 10.32877/bt.v7i3.2227.
[26] E. Mutiara, “Algoritma Klasifikasi Naive Bayes Berbasis Particle Swarm Optimization untuk Prediksi Penyakit Tuberculosis (TB),” *Jurnal Swabumi*, vol. 8, no. 1, pp. 46–58, 2020.
[27] B. R. Pratama, F. T. Anggraeny, and A. Junaidi, “Segmentasi Optic Cup dan Optic Disc Menggunakan U-Net Backbone ResNet50,” *JIP (Jurnal Informatika Polinema)*, vol. 11, no. 4, pp. 391–397, Aug. 2025.